NIH Public Access
Author Manuscript
Biomaterials. Author manuscript; available in PMC 2011 February 1.

Published in final edited form as:
Biomaterials. 2010 February ; 31(6): 1025–1035. doi:10.1016/j.biomaterials.2009.11.002.

Silk Nanospheres and Microspheres from Silk/PVA Blend Films for Drug Delivery

Xiaoqin Wang, **Tuna Yucel**, **Qiang Lu**, **Xiao Hu**, and **David L. Kaplan**
Department of Biomedical Engineering, Tufts University, 4 Colby Street, Medford, MA 02155, USA

Abstract

Silk fibroin protein-based micro- and nanospheres provide new options for drug delivery due to their biocompatibility, biodegradability and their tunable drug loading and release properties. In the present study, we report a new aqueous-based preparation method for silk spheres with controllable sphere size and shape. The preparation was based on phase separation between silk fibroin and polyvinyl alcohol (PVA) at a weight ratio of 1/1 and 1/4. Water-insoluble silk spheres were easily obtained from the blend in a three step process: (1) air-drying the blend solution into a film, (2) film dissolution in water and (3) removal of residual PVA by subsequent centrifugation. In both cases, the spheres had approximately 30% beta-sheet content and less than 5% residual PVA. Spindle-shaped silk particles, as opposed to the spherical particles formed above, were obtained by stretching the blend films before dissolving in water. Compared to the 1/1 ratio sample, the silk spheres prepared from the 1/4 ratio sample showed a more homogeneous size distribution ranging from 300 nm up to 20 μm. Further studies showed that sphere size and polydispersity could be controlled either by changing the concentration of silk and PVA or by applying ultrasonication on the blend solution. Drug loading was achieved by mixing model drugs in the original silk solution. The distribution and loading efficiency of the drug molecules in silk spheres depended on their hydrophobicity and charge, resulting in different drug release profiles. The entire fabrication procedure could be completed within one day. The only chemical used in the preparation except water was PVA, an FDA-approved ingredient in drug formulations. Silk micro- and nanospheres reported have potential as drug delivery carriers in a variety of biomedical applications.

Keywords

silk; fibroin; polyvinyl alcohol (PVA); nanospheres; microspheres; drug release

1. Introduction

Micro- and nanoparticulate systems have been widely used in biomedical and pharmaceutical applications [1]. For drug delivery purposes, these systems act as a reservoir of therapeutic agents, with spatial and temporal control of release profiles of the drug leading to desirable therapeutic outcomes. The micro- and nanoparticles used should have some general characteristics, such as the ability to incorporate the drug without loss of activity, tunable release kinetics, sufficient *in vivo* stability for function, biocompatibility in terms of lack of toxicity and immunogenicity, degradability and the potential to target specific organs and tissues. Depending on the delivery route and disease site, microspheres (1-1000 μm) or

Publisher's Disclaimer: This is a PDF file of an unedited manuscript that has been accepted for publication. As a service to our customers we are providing this early version of the manuscript. The manuscript will undergo copyediting, typesetting, and review of the resulting proof before it is published in its final citable form. Please note that during the production process errors may be discovered which could affect the content, and all legal disclaimers that apply to the journal pertain.

NIH-PA Author Manuscript
NIH-PA Author Manuscript
NIH-PA Author Manuscript

NIH-PA Author Manuscript

NIH-PA Author Manuscript

NIH-PA Author Manuscript

nanospheres (1-1000 nm) may be useful. Nanospheres can penetrate through small capillaries, across physiological barriers and incorporated into cells. Therefore, in recent years, significant effort has been devoted to develop drug-delivery nanospheres for treating various diseases such as cancer, due to the potential for more targeted localization in tumors with active cellular uptake [2].

Nanospheres are usually designed as short-acting delivery vehicles and administrated via intravenous, intramuscular, subcutaneous, oral, nasal, ocular or transdermal routes, either fluidized with a liquid carrier or as a solid powder [3,4]. Microspheres are more generally used as depot drug carriers for long-acting delivery and usually administered intramuscularly or subcutaneously [4]. Microspheres having mucoadhesive properties can also be delivered via oral or nasal routes to adhere to the mucous membrane and release encapsulated drug [4]. Drug release from nano- and microspheres is determined by the diffusion of drug molecules through the polymer network and/or material degradation. Long-acting delivery microvesicles can also be used for tissue regeneration by releasing growth factors from a polymeric scaffold [5]. Microvesicles can be incorporated in the scaffold and preferably distributed in a desired pattern so that the encapsulated growth factors are released in a spatial and temporal manner [6]. In some studies, nanospheres were incorporated into larger spheres by flocculation, spray drying, or other means, so that the spheres have a desired size to target a specific disease site, such as that in pulmonary drug delivery [7]. Nanospheres can also be microencapsulated using enteric coatings in order to control release and degradation *in vivo* [8]. It has also been reported that particle shape might also have significant impact on polymer degradation and, therefore, drug release profiles [9].

Both natural and synthetic materials can be used to fabricate micro- and nanoparticulate delivery systems. Most commonly used biodegradable synthetic polymers are polyesters and polyanhydrides [1]. Because these polymers are composed of one or two monomers, their *in vivo* degradation can be controlled and in some cases can be predicated by factors such as molecular weight, ratios between different monomers or copolymers, and degree of crystallinity. However, these polymers have some inherent shortcomings that may prevent broad applicability. For example, due to their hydrophobic nature, the polymers need to be dissolved in organic solvents that might be detrimental to protein drugs. Moreover, the degradation products are acidic, which can cause denaturation of protein drugs and loss of bioactivity. Compared with synthetic polymers, naturally derived degradable polymers, such as collagen, gelatin, cellulose, hyaluronic acid, alginate, and chitosan have good biocompatibility [1,10]. The obstacles to using natural polymers for biomedical applications are normally related to their inconstant batch qualities and uncontrollable degradation rates.

Silk fibroin proteins from *Bombyx mori*, the commercialized source of silk for textiles via sericulture, have been investigated as a biomaterial for tissue engineering and drug delivery [11-16]. Silk proteins represent a unique family of natural fibrous proteins due to their unique structure and resulting functions [11,17]. The molecular structure of many silks consists of large regions or domains of hydrophobic amino acids, segregated by relatively short and more hydrophilic regions. The hydrophobic domains organize into protein crystals, beta sheets, which form physical crosslinks to stabilize silk structures. These regions are dominated by repeats of alanine, glycine-alanine, or glycine-alanine-serine. The pI of silk is around 4, and most charged amino acids are located in the hydrophilic regions as well as in the N- and C-termini [18]. Compared to other natural degradable materials, silk fibroin exhibits superior mechanical properties, tunable degradation rates ranging from weeks to months *in vivo* due to control of crystallinity, excellent biocompatibility with low inflammatory and immunogenic response, diverse processing windows, and all aqueous material processing options to form films, fibers, gels, sponges and microspheres. For drug delivery, especially protein drugs, silk

NIH-PA Author Manuscript

NIH-PA Author Manuscript

NIH-PA Author Manuscript

materials exhibit high encapsulation efficiency and controllable drug release kinetics due to the control of crystalline beta-sheet formation [12,13].

There are several techniques available for the preparation of drug-loaded micro- and nanospheres, such as emulsion-solvent evaporation/extraction methods, solvent displacement, phase separation, self-assembly, rapid expansion of supercritical fluid solution, and spray drying. Each method has pros and cons, so that selection of an appropriate method is important in fabricating micro- and nanospheres for drug delivery applications. Although silk fibroin has been fabricated into microspheres by various means and used for drug delivery [13,16, 19-21], silk nanosphere fabrication remains a challenging area that needs further exploration. The high molecular weight and protein nature of silk make fabrication of nanospheres difficult to control, and more importantly, silk tends to self-assemble into fibers or gels upon exposure to heat, salt, pH change and high shear. The fabrication of silk nanospheres in a size range of 35-125 nm using at least 70% (v/v) water-miscible protonic and polar aprotonic organic solvents was reported [22]. Although the nanospheres prepared would be useful in cosmetics and anti-UV skincare products, they are not suitable for drug delivery applications due to the use of organic solvents. Moreover, the size and shape of the silk particles was not controllable. Therefore, for the delivery of labile and active molecules, a new strategy was desired to fabricate silk micro- and nanospheres with controllable sphere size and shape, and to avoid using organic solvents and any other harsh conditions during processing.

Phase separation between polyvinyl alcohol (PVA) and silk occurs spontaneously when the two polymer solutions are mixed and subsequently cast into films [23,24]. The influence of blending of PVA and silk on silk secondary structure changes as well as film mechanical and swelling properties was studied, and it was found that varying the molecular weight of PVA and the ratio between PVA and silk lead to a transition from macro- to microphase separation [23-26]. Based on these findings, the goal of the present study was to exploit the phase separation of silk/PVA blends to generate silk spheres with controlled micro- and nano-sphere size for utility in drug loading and release.

2. Materials and methods

2.1. Materials

Polyvinyl alcohol (PVA, average mol wt 30,000-70,000, 87-90% hydrolyzed), Rhodamine B, protease XIV, and all other chemicals used in the study were purchased from Sigma-Aldrich (St. Louis, MO). Tetramethylrhodamine conjugated bovine serum albumin (TMR-BSA) and Tetramethylrhodamine conjugated dextran (TMR-Dextran) are from Invitrogen (Carlsbad, CA). Ultrapure water from the Milli-Q system (Millipore) was used throughout this research.

2.2. Silk fibroin purification

Silk fibroin aqueous stock solutions were prepared as previously described [27]. Briefly, cocoons of *Bombyx mori* were boiled for 30 min in an aqueous solution of 0.02 M sodium carbonate, and then rinsed thoroughly with distilled water. After air-drying, the extracted silk fibroin was dissolved in 9.3 M LiBr solution at 60°C for 4 hours, yielding a 20% (w/v) solution. The solution was dialyzed against distilled water using Slide-a-Lyzer dialysis cassettes (MWCO 3,500, Pierce) for 3 days to remove the salt. The solution was centrifuged 2 times at 10,000 rpm for 20 min to remove silk aggregates as well as debris from original cocoons. The final concentration of silk fibroin aqueous solution was approximately 8% (w/v), based on weighing the residual solid of a known volume of solution after drying at 60°C. The 8% silk stock solution was stored at 4°C and diluted with ultrapure water before use.

NIH-PA Author Manuscript

NIH-PA Author Manuscript

NIH-PA Author Manuscript

2.3. Preparation of silk/PVA blend films

First, silk and PVA stock solutions were prepared at a concentration of 5 wt%. Blending was performed by gently mixing the silk and PVA stock solutions with the same initial concentration but different volumes in a glass beaker. In this manner, the final solute concentration in the blend due to silk and PVA was equal to the concentration of both silk and PVA stock solutions prior to blending, while the weight ratio of silk to PVA could be controlled by changing the volumetric ratio of each stock solution. For example, to obtain a blend with 5 wt% final solute concentration and a silk/PVA weight ratio of 1/4, typically 1 ml of 5 wt% silk solution was mixed with 4 ml of 5 wt% PVA solution. Similarly, to obtain a 5 wt% final solute concentration and a silk/PVA weight ratio of 1/1, typically 2.5 ml of silk solution was mixed with 2.5 ml of PVA solution. Lower concentration blends were prepared by diluting the silk and PVA stock solutions prior to mixing. In addition, the total silk and PVA mass in the blend solutions was kept constant regardless the blend concentration. For example, when blends were prepared from diluted stock solutions at concentrations of 1 or 0.2 wt%, the volume of solution used for blending was increased 5 and 250 times as compared to that of the 5 wt% solution, respectively. After mixing, the solution was stirred at 150 rpm for 2 h at room temperature, and then transferred to open polystyrene petri dishes having 35 mm, 100 mm, and 150 mm diameters for 5, 1 and 0.2 wt% concentration samples, respectively. With this approach the height of all samples in the petri dish was similar, leading to similar drying rates. All dishes were placed in a fume hood to dry overnight. Normally all the blend solutions dried within about 3 hours, forming films with a thickness of 70 to 100 μm. The dried films were then peeled off and stored in a sealed container at room temperature before use.

To study the sonication effects on the size of silk spheres, 1 ml of 5 wt% silk was mixed with 4 ml of 5 wt% of PVA (ratio 1/4) in a 15-ml conical tube and the blend solutions were then subjected to sonication using a Branson ultrasonic cell disruptor (model s-450D, Branson, Danbury, CT) at an energy output of 12% and 25% amplitude for 30 seconds, similar to conditions used in our previous silk gelation study [14]. The solution was immediately transferred to open 100×15 mm diameter petri dishes after sonication and dried overnight.

2.4. Preparation of silk nano- and microspheres

The dried silk/PVA blend films prepared from blend solutions were dissolved in 30 ml of ultrapure water in 50 ml centrifuge tubes with 10 min of gentle shaking at room temperature. The tubes were centrifuged in a Sorvall high speed centrifuge (Thermo Scientific, Waltham, MA) at 16,000 rpm, 4°C, 20 min. The supernatant was carefully discarded and the pellet was suspended in 30 ml of ultrapure water and centrifuged again. The final pellet was suspended in 2 ml of ultrapure water, sonicated at 10% amplitude for 15 seconds with a Branson ultrasonic cell disruptor to disperse the clustered silk spheres. The silk micro- or nanosphere suspension was characterized as described in the follow paragraphs.

2.5. Fourier transform infrared (FTIR) spectroscopy

The silk sphere suspensions in water prepared as above were lyophilized. The powder obtained as well as control samples of silk/PVA blend films prior to dissolution were subjected to FTIR measurement using a JASCO FTIR 6200 Spectrometer (JASCO, Tokyo, Japan) equipped with a MIRacle™ attenuated total reflection (ATR) Ge crystal cell in the reflection mode. Background signals were taken with an empty cell and subtracted automatically from the sample reading. Each sample was scanned 64 times from 400 to 4000 cm^{-1} with a resolution of 4 cm^{-1}. The fractions of secondary structures, including random coils, alpha-helices, beta-pleated sheets, and turns, were evaluated within the amide I region (1595-1705 cm^{-1}) using Fourier self-deconvolution software (Opus 5.0) provided by the manufacturer. The absorption bands shown in the frequency range of 1616-1637 cm^{-1} and 1695–1705 cm^{-1} represented enriched β-sheet structure in silk II form [28]. The absorption bands in the frequency range of

NIH-PA Author Manuscript

NIH-PA Author Manuscript

NIH-PA Author Manuscript

1638-1655 cm^{-1} were ascribed to random coil, 1656-1663 cm^{-1} ascribed to alpha-helices and 1663-1695 cm^{-1} to turns [28].

2.6. Differential scanning calorimetry (DSC)

Silk/PVA blend film samples with a weight about 5 mg were loaded in aluminum pans, which were then heated in a TA Instrument Q100 DSC (TA Instruments, New Castle, DE) with a dry nitrogen gas flow of 50 mL/min. Silk and PVA film alone served as a control. The instrument was calibrated for empty cell baseline and with indium for heat flow and temperature. Temperature-modulated differential scanning calorimetry (TMDSC) measurements were performed using a TA Instruments Q100, equipped with a refrigerated cooling system. The samples were heated at 2°C/min from -30°C to 350°C with a modulation period of 60s and temperature amplitudes of 0.318°C.

2.7. Scanning electron microscopy (SEM) and light microscopy

One hundred μl of the silk sphere suspension in water was directly added on top of a conductive tape mounted on a SEM sample stub. The samples were dried overnight in air and then sputtered with platinum. The morphologies of silk spheres were imaged using a Zeiss Supra 55 VP SEM (Carl Zeiss SMT, Peabody, MA). For light microscopy, either the cast blend film in a petri dish or a glass slide with 20 μl silk sphere suspension on top was placed under an inverted light microscope (Carl Zeiss, Jena, Germany). Images were taken with the installed software.

2.8. Dynamic light scattering (DLS)

DLS experiments were performed using a Brookhaven Instrument BI200-SM goniometer (Holtsville, NY) equipped with a diode laser operated at a wavelength, $\lambda = 532$ nm. All samples were filtered with a low protein binding, 5 μm membrane (Millex-SV, Millipore, Billerica, MA) prior to DLS measurements. The temperature was kept at 25°C with 0.05°C accuracy with a temperature-controlled recirculating bath. Scattered light intensity, I and the time-averaged autocorrelation function (ACF) of the scattered intensity, $g_2(q,t)$ were measured simultaneously using a Brookhaven cross-correlator to prevent possible after-pulsing effects at scattering angles (θ) between 30° and 150°. The relaxation of density fluctuations at wave vector, q and delay time, t was probed from $g_2(q,t)=\frac{\langle I(t)I(0)\rangle}{\langle I\rangle^2}$, where q is related to the refractive index of the solvent, n by $q=\frac{4\pi n}{\lambda}\sin(\frac{\theta}{2})$. When the system is ergodic, *i.e.* when a time-averaged measurement of a property gives a good estimate of its ensemble average, $g_2(t)$ is related to the normalized field correlation function, $g_1(q,t)$ by the Siegert relation:

$$g_2(q,t)=1+A^2 g_1(q,t)^2$$

where A is the instrumental coherence factor. The cumulative analysis of the DLS autocorrelation function was used to calculate the mean relaxation time, $\tau_{\bar{R}}$ and the polydispersity. Using the cumulative analysis parameters, an assumed Gaussian hydrodynamic diameter probability density, $G(D_h)$ and the hydrodynamic diameter cumulative distribution function, $C(D_h)$ could be plotted for qualitative visualization and comparison of data. More quantitative analysis of the distribution of relaxation times and corresponding size distributions could be obtained using the CONTIN method and exponential sampling. For the measurements reported here, both CONTIN and exponential sampling gave similar particle size distributions.

NIH-PA Author Manuscript

NIH-PA Author Manuscript

NIH-PA Author Manuscript

2.9. Determination of residual PVA content

During the preparation of silk spheres, the supernatant fractions from centrifugation were collected, and 1 ml of supernatant was diluted to 50 ml with ultrapure water. The diluted supernatants were subjected to PVA determination. To determine the residual PVA in the silk spheres, the spheres were lyophilized, and resuspended in 2 ml of freshly prepared protease XIV solution (1 mg/ml in PBS buffer, pH 7.4). The samples were incubated at 37°C for 15 h and the resulting solution was subjected to PVA determination directly. The amount of PVA in solution was determined as reported in the literature [29]. Briefly, 0.5 ml of sample solution was mixed with 3 ml of 0.65 M solution of boric acid and 0.5 ml of a solution of I_2/KI (0.05 M/0.25 M), and the volume was supplemented to 10 ml with ultrapure water. After 15 min incubation at room temperature, the samples were subjected to absorbance measurement at 690 nm. The amount of PVA was calculated based on a standard curve generated under the same conditions. The experiment was performed with N = 3 for each data point. Statistical analysis was performed by one-way analysis of variance (ANOVA) and Student-New-man-Keuls Multiple Comparisons Test. Differences were considered significant when $p \leq 0.05$, and very significant when $p \leq 0.01$.

2.10. Drug loading in silk spheres

Tetramethylrhodamine conjugated bovine serum albumin (TMR-BSA, MW = 66,000 Da), tetramethylrhodamine conjugated dextran (TMR-Dextran, MW = 10,000 Da), and rhodamine B (RhB, MW = 479 Da) were used as model drugs to study drug loading in the silk nano- and microspheres. Stock solutions with a concentration of 5 mg/ml in PBS buffer, pH 7.4, were first prepared and stored at -20°C. Before preparing silk nano- and microspheres, certain amounts of stock solutions were added to the silk solutions to reach a weight ratio of 1:100 between drug and silk. After mixing, the solution was used to blend with PVA solution following the steps described in the silk sphere preparation without sonication treatment. A 5 wt% polymer concentration and silk/PVA ratio of 1/4 was used in this study. Compared to the silk/PVA ratio of 1/1, the 1/4 ratio can generate silk spheres with narrower size distribution. In addition, the blend film is easier to dissolve in water forming homogeneous sphere suspension. To determine drug loading in the silk spheres, the supernatants collected from the centrifugation steps were subjected to absorbance measurement at 555 nm. The amount of drug was calculated based on a standard curve obtained at the same condition. The amount of drug in silk spheres was calculated from the difference between the total amount used and the amount remained in the supernatants. For each drug loading, at least three samples were prepared in order to obtain a standard deviation. The pellets from the last centrifugation step were suspended in 2 ml of PBS buffer, pH 7.4, and used for confocal microscopy and drug release studies.

2.11. Laser scanning confocal microscopy

The distribution of drug molecules in silk microspheres was investigated by confocal microscopy. The drug-loaded silk spheres were prepared and resuspended in PBS buffer, as described above. A small portion of the suspension was imaged using a 63×, 1.4 N.A. water immersion lens on a Leica DMIRE2 microscope (Welzlar, Germany) at an excitation wavelength of 555 nm and an emission wavelength of 580 nm. Either single *xy* scans were collected for sphere size determination or several *xy* scans with an optical slice of 1 μm were stacked along the z-direction to obtain a 3-*d* image and visualize the pore structure of silk spheres or the distribution of encapsulated drugs or proteins inside the spheres.

2.12. Drug release from silk spheres

Silk spheres loaded with model drugs were lyophilized, and 10 mg of lyophilized silk spheres were suspended in 1 ml of PBS buffer, pH7.4. The samples were incubated at 37°C with slow

NIH-PA Author Manuscript

NIH-PA Author Manuscript

NIH-PA Author Manuscript

shaking. At certain time points (1, 4, 8.5, 24, 48, 120, 192, 342 h), samples were centrifuged at 12,000 rpm for 10 min with a Sigma microcentrifuge (Model ISS-113), and the supernatants were carefully transferred to empty tubes and the pellets were suspended in 1 ml of PBS buffer to continue the release study. The collected supernatants were then subjected to absorbance measurements at 555 nm. The amount of model drug was then calculated based on a standard curve. The cumulative release was obtained by comparing the data with the original loading in the spheres. For each model drug, at least three samples were prepared in order to obtain statistical interpretations.

2.13. Zeta potential

To better understand different drug loading and release properties, surface charges of the silk spheres were determined via Zeta potential measurements. Silk spheres prepared from a silk/PVA (1/4) blend film were suspended in ultrapure water, yielding a concentration of about 100 μg/ml. One ml of the solution was then loaded to a zeta potential analyzer (Zetasizer nano, Malvern, Westborough, MA) for the zeta potential measurement at 25 °C.

3. Results and discussion

3.1. Characterization of silk nano- and microspheres

Silk/PVA blend films have been characterized in terms of mechanical properties, swelling, and permeability [23-25]. It has been noticed that silk and PVA were macroscopically or microscopically separated into different phases in the blend films, and the phase separation was dependent on the ratio between silk and PVA as well as the molecular weight of PVA used. When silk fibroin was less than 50 wt% in the blend film, microspheres formed with size distributions from less than 1 μm to approximately 30 μm [23]. In the present study, we further investigated these blend films in order to prepare silk micro- and nanospheres under mild, aqueous and relatively simple conditions.

Silk and PVA solutions with a 5 wt% concentration were mixed at a volumetric ratios of 1/1 and 1/4, and then cast into films. When the blend film was dissolved in water, it was found that the silk microspheres retained their original spherical shape and size (1-30 micrometers), and could be readily spun down and resuspended. Under SEM, both 1/1 and 1/4 silk/PVA samples contained micro- and nanospheres with rough surfaces containing nanometer-sized pores (Figure 1A,B). The 50% methanol treatment did not result in a change on the morphology of the spheres (Figure 1C). When the spheres were washed two times with water (spheres were normally washed once), the surface became rougher and showed more pores, due to the more complete removal of the PVA (Figure 1D). The nanofibrillar interior structure of the spheres could be observed through occasional surface defects (Figure 1D inset). Such surface morphology and interior porous structure might provide the silk spheres with unique drug loading and release properties.

Comparing the Silk/PVA blend films with ratio of 1/1 and 1/4, the latter could quickly, within 10 min, dissolve in water forming a homogeneous suspension, and the microspheres formed had a narrower size distribution when compared to the former, as observed by both light microscopy and SEM (data not shown). In a control experiment, when a silk/PVA blend solution was stirred for 2 hours at room temperature (the same condition used to prepare blend films) followed by immediate centrifugation, silk microspheres could not be spun down and instead formed a pellet. Therefore, drying the blend solution into a film was an essential step for the formation of stable water-insoluble silk nano- and microspheres. In our previous studies, methanol (or ethanol) and water vapor (water-annealing) treatments are two commonly used methods to increase beta-sheet content in an as-cast silk film, making it water-insoluble [30]. In the present study, when methanol was directly added to the silk/PVA blend solutions to

NIH-PA Author Manuscript

NIH-PA Author Manuscript

NIH-PA Author Manuscript

reach a methanol concentration higher than 50% (v/v), water-insoluble silk nano- and microspheres accompanied with many silk fibrillar aggregates also formed (Figure 1E). These types of aggregates were not observed in the blend film preparation. When the silk/PVA blend films were treated with water vapor under a vacuum environment for 24 h at room temperature, the films were still soluble in water, and some of the silk spheres formed exhibited a wrinkled surface (Figure 1F) and/or a flattened disk shape (Figure 1G). Interestingly, when the silk/PVA blend films were stretched by hand before dissolving in water, the shape of the silk spheres, particularly those with micrometer sizes, became elongated, forming a spindle-like morphology instead of spheres (Figure 1 H,I). Some spheres were damaged during stretching, revealing the interior porous structure (Figure 1H inset). The spindle-shaped particles retained their shape when the stretched blend films were treated with either 50% (v/v) methanol or water vapor prior to dissolving in water (data not shown). Therefore, applying physical forces, such as stretching, can irreversibly change the shape of silk particles in the blend films. We envision that applying other forces, such as compression and twisting, can generate silk particles with different shapes, a novel feature of this new processing approach. Changes in silk particle shape may significantly change *in vivo* degradation and drug release behavior, as suggested in the literature [7].

To determine the beta-sheet content, FTIR was performed on both silk/PVA blend films (1/1 and 1/4 ratio) prior to dissolution and the lyophilized silk spheres prepared from the same blend films with different treatments, such as direct dissolution, water vapor-treatment (water-annealing), and stretching. As a high beta-sheet content control, the spheres prepared from methanol-treated silk/PVA blend solutions were also measured. In previous studies with silk films, it was found that the as-cast films initially exhibited a mostly amorphous structure (1538 cm^{-1}) with some silk I structure (1658, 1652 cm^{-1}). After water-annealing treatment, the silk I structure was predominant, while after methanol treatment the silk II content (1697, 1627, 1528 cm^{-1}) increased with the formation of more than 50% beta-sheet [30]. Once significant amount of silk I structure (about 30% beta-sheet) formed, further methanol treatment could not convert the structure to silk II [30]. In the present study, the silk spheres from the methanol-treated blend solution had approximately 50% beta-sheet (silk II), whereas those from directly dissolved blend films had about 30% beta-sheet content (silk I) (Table 1). The blend films prior to water dissolution, however, showed different beta-sheet contents. The 1/1 blend film showed a 27% silk beta-sheet content, similar to that measured for the spheres after film dissolution, while the 1/4 blend film had only 20% beta-sheet (Table1). Apparently, similar to the role of water vapor on silk films, PVA promoted the formation of the silk I structure in the 1/1 blend film, probably due to hydrogen bonding formed between hydroxyl groups of PVA and silk. In the case of the 1/4 blend film, the presence of PVA at high concentration perhaps restricted the silk structural transition from amorphous to silk I, due to more extensive hydrogen bonds formed between silk and PVA. During film dissolution, a decrease in local PVA concentration led to reduced hydrogen bonding between silk and PVA, and as a result, the transition from amorphous to silk I structure could occur. The intermolecular interactions between silk and PVA in different blend films were demonstrated by the DSC data. As shown in Figure 2, the glass transition temperatures (Tg) for silk and PVA in the 1/4 blend film did not significantly change when compared to the control samples, silk and PVA film alone (22 and 55 °C, respectively). It has been reported that the Tg of silk film is stable when bound water is plasticized in the sample [30]. This indicates that the intermolecular interactions between silk and PVA, though restricting silk structural transitions as discussed above, did not significantly change the material properties for the PVA and silk separated phases in the blend film. For the 1/1 blend film, the silk Tg did not significantly change but the Tg for PVA shifted toward silk to 35°C (Figure 2), indicating that intermolecular interactions between silk and PVA reached a state such that PVA properties were changed. Meanwhile, the interaction also induced a silk structural transition to silk I, but failed to induce a significant shift in Tg. This is possibly because the shift of the silk Tg only occurs only with silk II (beta-sheets crystal) structure

NIH-PA Author Manuscript

NIH-PA Author Manuscript

NIH-PA Author Manuscript

formation [28,31]. Evidence was shown in the silk/PVA (1/4) blend and sonicated film, in which the Tg for PVA and silk component increased to 37°C and 70°C, respectively (Figure 2). As revealed by FTIR, the beta-sheet content in the same film was 42%, much higher that the 19% content in the film without sonication (Table 1).

It has been known that higher silk II content may result in slower enzymatic hydrolysis of the silk material [30]. Therefore, the silk spheres prepared from silk/PVA blend films that exhibit less crystalline-silk II content (less than 30%) would be expected to have faster *in vitro* and *in vivo* degradation rates than those prepared by methanol treatment [12,13]. This will provide alternative options in future drug delivery options in which different material degradation rates are useful.

Residual PVA content in the silk spheres was determined using protease XIV to digest silk spheres and release residual PVA [32]. As shown in Figure 3, less than 5 wt% PVA remained in all silk spheres, and the result was confirmed by the PVA content determined in the supernatants. Since PVA is a FDA approved ingredient widely used in oral and intraocular drug formulation, low amounts of residual PVA should not affect future biomedical applications.

3.2. Control of sphere size

Silk spheres prepared from blend films are heterogeneous in size, from nanometers to micrometers. To obtain more homogeneous micro- or nanospheres, two strategies were employed to control silk phase separation in PVA solution: (1) Dilution to reduce the number of hydrogen bonds formed between silk and PVA or (2) sonication of the blend solution to break down large silk macro- or microphases via application of high energy to the blend system.

We first tested the effect of varying polymer concentrations by dilution on particle sizes. In this experiment, the concentration of silk and PVA in blend solution was decreased progressively from 5 wt% to 1 and 0.2 wt%, while keeping the weight ratio of silk and PVA constant at 1/4. Under SEM, there was no significant improvement for the 5 and 1 wt% samples, while the 0.2 wt% sample was dominated by nanospheres with a relatively homogeneous size distribution (100–500 nm) (Figure 4). To observe the *in situ* particle size in the hydrated state, samples were subjected to DLS. Prior to DLS measurements, silk sphere suspensions in water were filtered through a 5 μm membrane. Figure 5 (a) compares the sphere hydrodynamic diameter distributions (as probability densities, $G(D_h)$ and cumulative distribution functions, $C(D_h)$) obtained using the cumulative analysis for easy comparison of data collected from 5 wt% and 0.2 wt% preparations. Figure 5 (b) provides more quantitative size distributions obtained using exponential sampling (CONTIN analysis results gave similar diameter distributions and therefore not plotted for ease of visualization) for the same samples as in Figure 5 (a). Cumulative analysis of DLS data collected from the 0.2 wt% sample showed a relatively homogeneous size distribution with a mean sphere size of 452 nm, and a polydispersity index (PDI) of 0.29, with no apparent sphere size larger than 2 μm (Figure 5). The 1 wt% (data not shown) and 5 wt% samples, however, had larger mean sizes (536 and 578 nm, respectively) and PDI values (0.56 and 0.68, respectively), and a broad sphere size distribution ranging from 100 nm to 5 μm (Figure 5). The average sphere hydrodynamic diameters and polydispersities obtained using DLS cumulant analysis are summarized in Table 2. These results are consistent with the SEM data, confirming a decrease in the average particle size with decreasing concentration. Therefore, combined DLS and SEM data demonstrated that the formation of hydrogen bonding between silk and PVA hydroxyl groups could stabilize silk spheres, while changing the polymer concentrations could alter silk/PVA interactions, and thus control average sphere size and size distribution. Based on reports in literature on blend films [26], using PVA with different molecular weights could also change the mean sphere size and size distribution. However, when we repeated the above experiment with a higher

NIH-PA Author Manuscript

NIH-PA Author Manuscript

NIH-PA Author Manuscript

molecular weight PVA (M.W. = 146,000-186,000), the blend films were not soluble in water, even after relatively long time frames (several days) of incubation at room or high (60°C) temperature. Future studies will focus on lowering the nanosphere size below 300 nm. One of the strategies would be mixing the silk/PVA solution with another –OH rich compound, such as glycerin, in order to influence the interaction between PVA and silk and, therefore, the phase separation [33].

To demonstrate the effect of energy input on silk/PVA phase separation, the solution was subjected to ultrasonication prior to film casting. In this experiment, silk and PVA concentrations were 5 wt% and the weight ratio was 1/4. When 12 and 25% of maximal sonication energy output (corresponding to 4 and 8 watts, respectively) were used, light microscopy indicated that the cast silk/PVA blend films were dominated by microspheres and nanospheres, respectively (Figure 6). Apparently, the 12% amplitude energy output could only break down larger microspheres, resulting in smaller microspheres with a size range of 5–10 μm. The possible presence of smaller nanospheres after 12% sonication could not be studied by light microscopy due to resolution limitations. The 25% amplitude energy, however, was high enough to break most spheres down to nanometer size. DLS measurements confirmed the light microscopy observations and provided additional information about the presence of nanospheres in sonicated samples. Figure 5 (a,b) give cumulant and exponential sampling results obtained from 25% amplitude sonicated samples, as mentioned previously for the concentration series. Cumulant analysis of DLS data collected from the 25% amplitude treated sample gave a mean sphere size of 322 nm, a PDI of 0.4, and no spheres larger than 2 μm. The 12% amplitude sample also contained similar sized nanospheres, but the static light scattering intensity was approximately 4 times lower than that of the 25% amplitude sample (data not shown). Considering the same initial silk/PVA concentrations were used prior to sonication, the lower scattered intensity from the 12% amplitude sample when compared to the 25% amplitude sample was attributable to the filtering of several-micron-sized spheres observed by light microscopy during DLS sample preparation of 12% sonicated samples. Therefore, changing sonication energy output, i.e., energy input in the blend solution, can effectively control the average size and size distribution of silk spheres covering both micro- and nanometer ranges. For future preparations requiring pure silk microspheres, silk nanospheres could easily be removed from the microsphere population by filtration or centrifugation. The beta-sheet content in the silk spheres prepared by 25% amplitude sonication was determined by FTIR. The result showed a significant increase of beta-sheet formation, approximately 12%, when compared to the silk spheres without sonication treatment, indicating the formation of crystal silk II structure in this case (Table 1). Interestingly, the sonicated silk in the blend film prior to dissolution showed a low beta-sheet content, 19%, similar to that in the as-cast film and silk solution, indicating that the crystal silk II structure formation only occurred during the film dissolution process but not during or after sonication and film drying. It has been known that applying similar amounts of sonication energy to silk solutions can induce silk gelation and was accompanied with significant increase of beta-sheet structure [14]. Apparently, similar to that observed in the silk/PVA 1/4 film without sonication, the strong intermolecular interactions between silk and PVA also restricted the silk structural transition from amorphous to silk II structure. The intermolecular interactions in this case were more extensive and stronger, so that the Tg for both silk and PVA shifted toward higher temperatures, as revealed by DSC measurement (Figure 2).

3.3. Yield and stability

The yield of silk nano- and microspheres prepared from 1/4 silk/PVA sample was estimated based on the mass balance after lyophilization. It was found that the yield was about 50-60% for the 25% amplitude-sonicated sample, 30-40% for the 12% sonicated sample and less than 20% for the non-sonicated sample. The stability of the sphere suspension, as observed during

NIH-PA Author Manuscript

NIH-PA Author Manuscript

NIH-PA Author Manuscript

sample storage at 4°C for up to 3 months, followed a similar trend to the yield, with the 25% sonicated sample more stable than the others. A small portion of the nanospheres in the 25% sonicated sample precipitated during storage, which, they could be readily resuspended by shaking. The microspheres in the 12% sonicated and non-sonicated sample, however, precipitated within a few days, forming a dense pellet. After being stored for more than a week, the samples had to be sonicated again to obtain individual microspheres. It is likely the silk spheres prepared under different sonication conditions had different mechanical properties, due to the beta-sheet contents in the spheres, resulting in different yields and stability.

3.4. Drug loading and release properties

As a model drug, tetramethylrhodamine conjugated bovine serum albumin (TMR-BSA), tetramethylrhodamine conjugated dextran (TMR-Dextran) and rhodamine B (RhB) were mixed with silk (1/100 weight ratio) prior to blending with PVA. Rhodamine emits red fluorescence after excitation so that the distribution of conjugated drug molecules in silk microspheres can be monitored and their loading and release readily determined. The three model drugs have different molecular weights (66,000, 10,000, 479 Da, respectively), hydrophobicities (RhB > TMR-BSA > TMR-Dextran) and surface charge (RhB: positive, TMR-BSA: negative, TMR-Dextran: neutral), leading to differences in drug distribution, loading and release. RhB-loaded silk spheres emitted strong red fluorescence and no structural details could be identified (Figure 7 C,F). The loading efficiency was approximately 95%. RhB has both hydrophobic and positively charged moieties, both of which might contribute to the strong binding of RhB to silk via hydrophobic interactions and electrostatic attraction (the zeta potential for the silk spheres were measured as -20 mV), resulting in a high loading efficiency and a slow release profile. Under confocal laser scanning microscopy, TMR-BSA-loaded spheres showed a porous structure with pores separated by red fluorescent fibers, similar to the porous structure observed by SEM (compare Figure 7A,D and Figure 1C). It is likely that the red fluorescent fibers were silk fibers associated with TMR-BSA. The strong interaction between TMR-BSA and silk fibers prevented TMR-BSA from diffusing into the surrounding medium during silk sphere preparation. The loading efficiency of TMR-BSA was determined to be about 51% (Figure 7). TMR-dextran-loaded spheres showed weak red fluorescence background decorated by some strong red fluorescent aggregates (Figure 7 B,E). It seems that TMR-dextran exist as either single molecules or aggregates and are distributed evenly in the silk spheres with no strong association with silk fiber structures. The loading efficiency of TMR-dextran was approximately 1.2%, much less than that of TMR-BSA. Apparently most TMR-dextran was extracted during silk sphere preparation, due to the weaker binding of dextran to silk material. The lower molecular weight of dextran when compared to BSA might also have contributed to the low drug loading efficiency due to faster molecule diffusion from the spheres. Overall, the strong binding of RhB with silk was presumably due to strong electrostatic and hydrophobic interactions. The negative charge and reduced hydrophobic interactions between silk and BSA possibly leads to lower binding than that of RhB, while the hydrophilic nature of the dextran molecule apparently dictated its low binding affinity to silk.

The drug release profiles turned out to be a compromise between the silk-drug interaction and the drug molecular weight. Following a short and low-level (about 1%) initial burst release, probably due to the release of residual drug that remained on or near the surface of silk spheres, the TMR-BSA and RhB were released slowly, with less than 5% of total loading being released within 2 weeks (Figure 8). In contrast, TMR-dextran was released much faster, with more than 60% of total loading being released within 2 weeks at a nearly zero-order release rate (Figure 8). Since the molecular weight of RhB is much lower than that of TMR-BSA and TMR-dextran, the results indicate that the interaction between silk and encapsulated drug, rather than the diffusion, controlled the drug release.

NIH-PA Author Manuscript

NIH-PA Author Manuscript

NIH-PA Author Manuscript

Thus, similar to phospholipids, the characteristic amphiphilic nature of silk molecules facilitates the loading of both hydrophobic and hydrophilic drugs in silk spheres due to intermolecular interactions, with potential to control drug loading and release by varying the degree of silk crystallinity (beta-sheet structure formation) in the hydrophobic regions and/or the charge states in the hydrophilic regions. Compared to widely used lipid vesicles, due to their high molecular weight, amino acid composition and unique structure, silk vesicles are more chemically and physically stable and more suitable for delivering macromolecular drugs. Other silk fibroin-based drug delivery systems have been widely reported in the literature, such as films, porous sponges, ultrathin coatings and nanofibers (Table 3). These delivery systems were mainly studied for growth factors and cells for tissue engineering. The silk particles reported in the present study, based on the ability to control size and shape, can be incorporated in these systems and used as reservoir carriers for growth factors, providing a more sustained and controlled release. Spatial and temporal patterning of growth factors can also be achieved by incorporating silk nano-/microparticles in the systems. Silk microspheres and nanospheres prepared with different methods have also been reported (Table 3). Compared to these systems, the present study provides a unique method that can control the size and shape of the particles according to specific requirements. The method requires no organic solvents and no expensive equipment during material processing, therefore, this is a green technology suitable for the future biomedical and pharmaceutical applications for drug delivery.

4. Conclusions

Silk micro- and nanospheres with controllable sizes and changeable shapes could be prepared using PVA as a continuous phase to separate silk solution into micro- and nanospheres in silk/PVA blend films at a weight ratio from 1/1 to 1/4, with the latter yielding more homogeneous spheres. Water-insoluble and beta-sheet-increased silk micro- or nanospheres could be easily obtained by film dissolution and subsequent centrifugation to remove PVA, and the spindle-shaped microspheres could be obtained by simply stretching the blend films. Varying silk and PVA concentration or applying ultrasonication to the blend solution was able to control sphere size and distribution. The porous interior space and amphiphilic nature of silk micro- or nanospheres facilitated the entrapment of drugs with different molecular weights and hydrophobicities, making drug release controllable. The reported preparation method is easy and safe to manipulate, time and energy efficient, and amenable to a wide range of drugs, and thus should be useful for silk-based drug delivery systems.

Acknowledgments

We thank the NIH P41 Tissue Engineering Resource Center (P41 EB002520) for support of this work.

References

1. Chiellini F, Piras AM, Errico C, Chiellini E. Micro/nanostructured polymeric systems for biomedical and pharmaceutical applications. Nanomed 2008;3:367–93.
2. Davis ME, Chen Z, Shin DM. Nanoparticle therapeutics: An emerging treatment modality for cancer. Nat Rev Drug Discov 2008;7:771–82. [PubMed: 18758474]
3. Hoet PH, Brüske-Hohlfeld I, Salata OV. Nanoparticles - known and unknown health risks. J Nanobiotechnology 2004;2:1–15. [PubMed: 14715086]
4. Mundargi RC, Babu VR, Rangaswamy V, Patel P, Aminabhavi TM. Nano/micro technologies for delivering macromolecular therapeutics using poly(d,l-lactide-co-glycolide) and its derivatives. J Control Release 2008;125:193–209. [PubMed: 18083265]
5. Chen RR, Mooney DJ. Polymeric growth factor delivery strategies for tissue engineering. Pharm Res 2003;20:1103–12. [PubMed: 12948005]

NIH-PA Author Manuscript

NIH-PA Author Manuscript

NIH-PA Author Manuscript

6. Wang X, Wenk E, Zhang X, Meinel L, Vunjak-Novakovic G, Kaplan DL. Growth factor gradients via microsphere delivery in biopolymer scaffolds for osteochondral tissue engineering. J Control Release 2009;134:81–90. [PubMed: 19071168]
7. Rytting E, Nguyen J, Wang X, Kissel T. Biodegradable polymeric nanocarriers for pulmonary drug delivery. Expert Opin Drug Deliv 2008;5:629–39. [PubMed: 18532919]
8. Lee KE, Cho SH, Lee HB, Jeong SY, Yuk SH. Microencapsulation of lipid nanoparticles containing lipophilic drug. J Microencapsul 2003;20:489–96. [PubMed: 12851049]
9. Champion JA, Katare YK, Mitragotri S. Particle shape: a new design parameter for micro- and nanoscale drug delivery carriers. J Control Release 2007;121:3–9. [PubMed: 17544538]
10. Dang JM, Leong KW. Natural polymers for gene delivery and tissue engineering. Adv Drug Deliver 2006;58:487–99.
11. Altman GH, Diaz F, Jakuba C, Calabro T, Horan RL, Chen J, et al. Silk-based biomaterials. Biomaterials 2003;24:401–16. [PubMed: 12423595]
12. Hofmann S, Foo CT, Rossetti F, Textor M, Vunjak-Novakovic G, Kaplan DL, et al. Silk fibroin as an organic polymer for controlled drug delivery. J Control Release 2006;111:219–27. [PubMed: 16458987]
13. Wang X, Wenk E, Matsumoto A, Meinel L, Li C, Kaplan DL. Silk microspheres for encapsulation and controlled release. J Control Release 2007;117:360–70. [PubMed: 17218036]
14. Wang X, Kluge JA, Leisk GG, Kaplan DL. Sonication-induced gelation of silk fibroin for cell encapsulation. Biomaterials 2008;29:1054–64. [PubMed: 18031805]
15. Yucel T, Cebe P, Kaplan DL. Vortex-induced silk fibroin hydrogels. Biophys J 2009;97:2044–50. [PubMed: 19804736]
16. Wenk E, Wandrey AJ, Merkle HP, Meinel L. Silk fibroin spheres as a platform for controlled drug delivery. J Control Release 2008;132:26–34. [PubMed: 18761384]
17. Kaplan, DL.; Adams, W.; Farmer, B.; Viney, C. Silk polymers: materials science and biotechnology. Washington D.C.: American Chemical Society; 1994.
18. Bini E, Knight DP, Kaplan DL. Mapping domain structures in silks from insects and spiders related to protein assembly. J Mol Biol 2004;335:27–40. [PubMed: 14659737]
19. Hino T, Shimabayashi S. Silk microspheres prepared by spray-drying of an aqueous system. Pharmacy Pharmacol Commun 2000;6:335–9.
20. Gobin AS, Rhea R, Newman RA, Mathur AB. Silk-fibroin-coated liposomes for long-term and targeted drug delivery. Int J Nanomedicine 2006;1:81–7. [PubMed: 17722265]
21. Wang X, Wenk E, Hu X, Castro GR, Meinel L, Wang X, et al. Silk coatings on PLGA and alginate microspheres for protein delivery. Biomaterials 2007;28:4161–9. [PubMed: 17583788]
22. Zhang YQ, Shen WD, Xiang RL, Zhang LJ, Gao WJ, Wang WB. Formation of silk fibroin nanoparticles in water-miscible organic solvent and their characterization. J Nanoparticle Res 2007;9:885–900.
23. Yamaura K, Kuranuki N, Suzuki M, Tanigami T, Matsuzawa S. Properties of mixtures of silk fibroin/syndiotacti-rich poly (vinyl alcohol). J Appl Polym Sci 1990;41:2409–25.
24. Tanaka T, Suzuki M, Kuranuki N, Tanigami T, Yamaura K. Properties of silk fibroin/poly(vinyl alcohol) blend solutions and peculiar structure found in heterogeneous blend films. Polym Int 1997;42:107–11.
25. Liu Y, Liu H, Qian J, Deng J, Yu T. Structure and properties of the composite membrane of regenerated silk fibroin and PVA and ITS application to amperometric tetrathiafulvalene-mediating glucose sensor. J Macromol Sci: Pure Appl Chem 1996;33:209–19.
26. Tanaka T, Tanigami T, Yamaura K. Phase separation structure in poly(vinyl alcohol)/silk fibroin blend films. Polym Int 1998;45:175–84.
27. Sofia S, McCarthy MB, Gronowicz G, Kaplan DL. Functionalized silk-based biomaterials for bone formation. J Biomed Mater Res 2001;54:139–48. [PubMed: 11077413]
28. Hu X, Kaplan DL, Cebe P. Determining beta-sheet crystallinity in fibrous proteins by thermal analysis and infrared spectroscopy. Macromolecules 2006;39:6161–70.

NIH-PA Author Manuscript

NIH-PA Author Manuscript

NIH-PA Author Manuscript

29. Abdelwahed W, Degobert G, Fessi H. A pilot study of freeze drying of poly(epsilon-caprolactone) nanocapsules stabilized by poly(vinyl alcohol): formulation and process optimization. Int J Pharm 2006;309:178–88. [PubMed: 16326053]
30. Jin HJ, Park J, Karageorgiou V, Kim UJ, Valluzzi R, Cebe P, et al. Water-stable silk films with reduced β-sheet content. Adv Funct Mater 2005;15:1241–7.
31. Hu X, Kaplan DL, Cebe P. Dynamic protein-water relationships during beta sheet formation. Macromolecules 2008;41:3939–48.
32. Horan RL, Antle K, Collette AL, Wang Y, Huang J, Moreau JE, et al. In vitro degradation of silk fibroin. Biomaterials 2005;26:3385–93. [PubMed: 15621227]
33. Dai L, Li J, Yamada E. Effect of glycerin on structure transition of PVA/SF blends. J Appl Polym Sci 2002;86:2342–7.
34. Wilz A, Pritchard EM, Li T, Lan JQ, Kaplan DL, Boison D. Silk polymer-based adenosine release: Therapeutic potential for epilepsy. Biomaterials 2008;29:3609–16. [PubMed: 18514814]
35. Numata K, Subramanian B, Currie HA, Kaplan DL. Bioengineered silk protein-based gene delivery systems. Biomaterials 2009;30:5775–84. [PubMed: 19577803]
36. Gupta V, Aseh A, Ríos CN, Aggarwal BB, Mathur AB. Fabrication and characterization of silk fibroin-derived curcumin nanoparticles for cancer therapy. Int J Nanomedicine 2009;4:115–22. [PubMed: 19516890]
37. Zhang YQ, Xiang RL, Yan HB, Chen XX. Preparation of silk fibroin nanoparticles and their application to immobilization of L-asparaginase. Gaodeng Xuexiao Huaxue Xuebao/Chemical Journal of Chinese Universities 2008;29:628–33.
38. Uebersax L, Mattotti M, Papaloïzos M, Merkle HP, Gander B, Meinel L. Silk fibroin matrices for the controlled release of nerve growth factor (NGF). Biomaterials 2007;28:4449–60. [PubMed: 17643485]
39. Wang X, Hu X, Daley A, Rabotyagova O, Cebe P, Kaplan DL. Nanolayer biomaterial coatings of silk fibroin for controlled release. J Control Release 2007;121:190–9. [PubMed: 17628161]
40. Bayraktar O, Malay O, Özgarip Y, Batigün A. Silk fibroin as a novel coating material for controlled release of theophylline. Eur J Pharm Biopharm 2005;60:373–81. [PubMed: 15996578]
41. Wang X, Zhang X, Castellot J, Herman I, Iafrati M, Kaplan DL. Controlled release from multilayer silk biomaterial coatings to modulate vascular cell responses. Biomaterials 2008;29:894–903. [PubMed: 18048096]
42. Karageorgiou V, Tomkins M, Fajardo R, Meinel L, Snyder B, Wade K, Chen J, Vunjak-Novakovic G, Kaplan DL. Porous silk fibroin 3-D scaffolds for delivery of bone morphogenetic protein-2 in vitro and in vivo. J Biomed Mater Res A 2006;78:324–34. [PubMed: 16637042]
43. Uebersax L, Merkle HP, Meinel L. Insulin-like growth factor I releasing silk fibroin scaffolds induce chondrogenic differentiation of human mesenchymal stem cells. J Control Release 2008;127:12–21. [PubMed: 18280603]
44. Li C, Vepari C, Jin HJ, Kim HJ, Kaplan DL. Electrospun silk-BMP-2 scaffolds for bone tissue engineering. Biomaterials 2006;27:3115–24. [PubMed: 16458961]

NIH-PA Author Manuscript
NIH-PA Author Manuscript
NIH-PA Author Manuscript

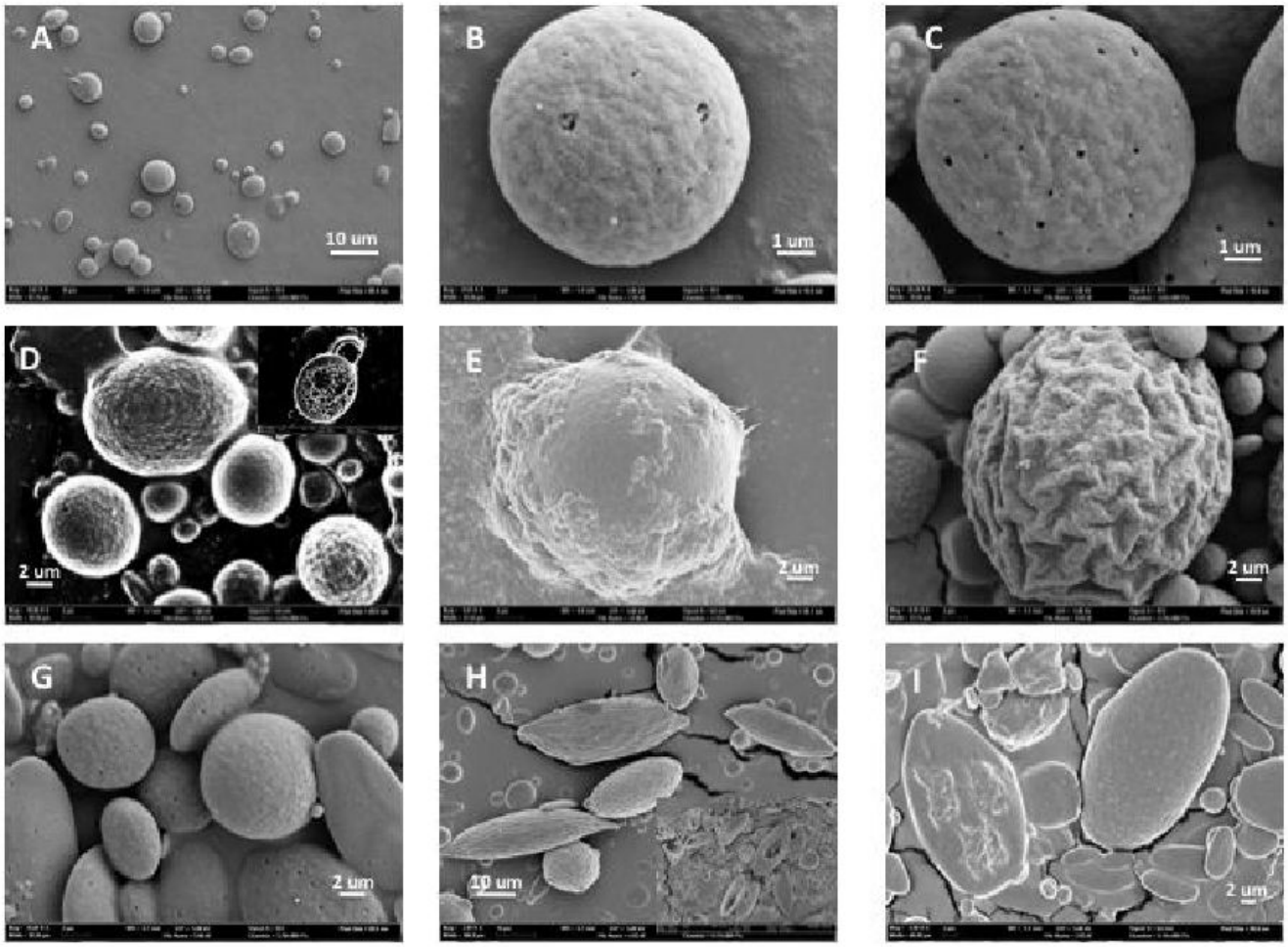

Figure 1.

Scanning electron microscopic images of silk particles prepared from 1/4 silk/PVA blend films. A-D, silk micro- and nanospheres prepared after film dissolution, centrifugation, washing and drying steps. Spheres were washed one time after film dissolution in A&B, washed one time followed by 50% MeOH treatment for 24 h in C, and washed three times in D. The inset in D showed a silk microsphere with an interior porous structure. E, silk microspheres prepared by mixing 1/4 silk/PVA blend solution with 50% (v/v) methanol for 15 h. The spheres were centrifuged and washed once with water.. F, G, silk spheres prepared from water-annealed blend films. H, I, spindle-shaped silk particles prepared from stretched blend films. Scale bar = 10 μm in A and H to show multiple particles in general. Bar = 1 μm in B,C&D and 2 μm in E,F&G to show the detailed surface morphology of individual particles.

NIH-PA Author Manuscript

NIH-PA Author Manuscript

NIH-PA Author Manuscript

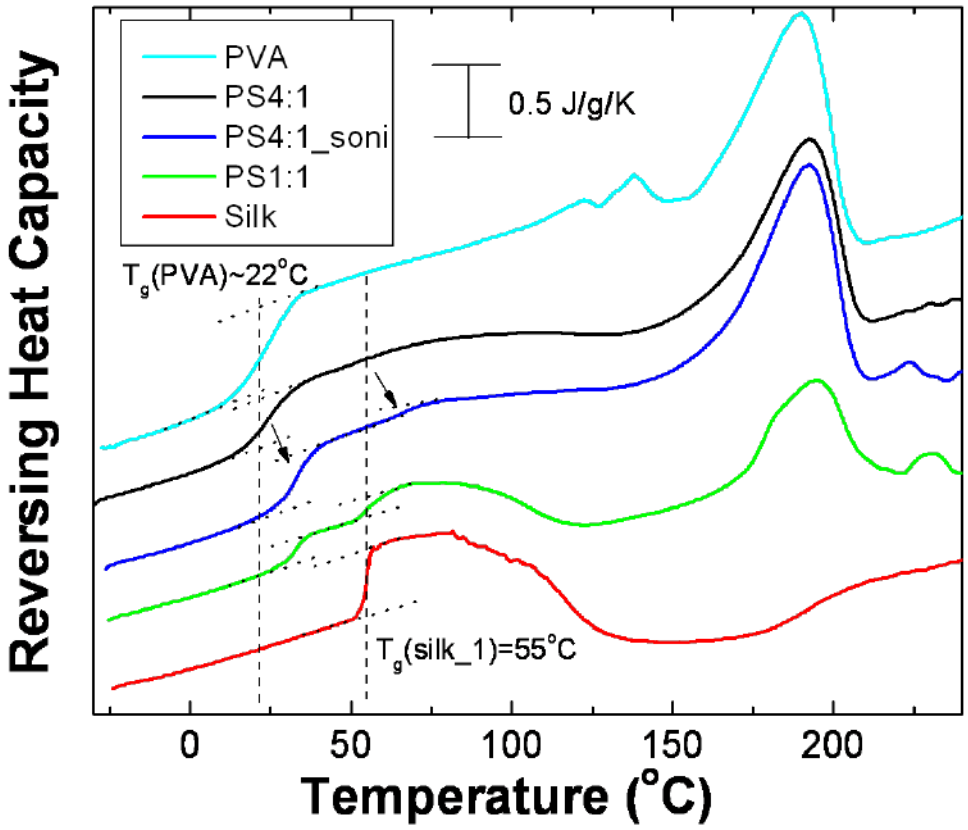

Figure 2.

DSC measurement on silk/PVA blend films. PS = PVA and silk. For the silk/PVA 1/1 blend film (green line), the glass transition (Tg) of PVA shifted higher (pink arrow), while that of silk did not change (red arrow). For the silk/PVA 1/4 blend film (black line), the Tg for both PVA and silk did not change. For the silk/PVA 1/4 blend and sonicated film (blue line), the Tg for both PVA and silk shifted higher (black arrows). PVA (turquoise line) and silk film (red line) alone served a control.

NIH-PA Author Manuscript
NIH-PA Author Manuscript
NIH-PA Author Manuscript

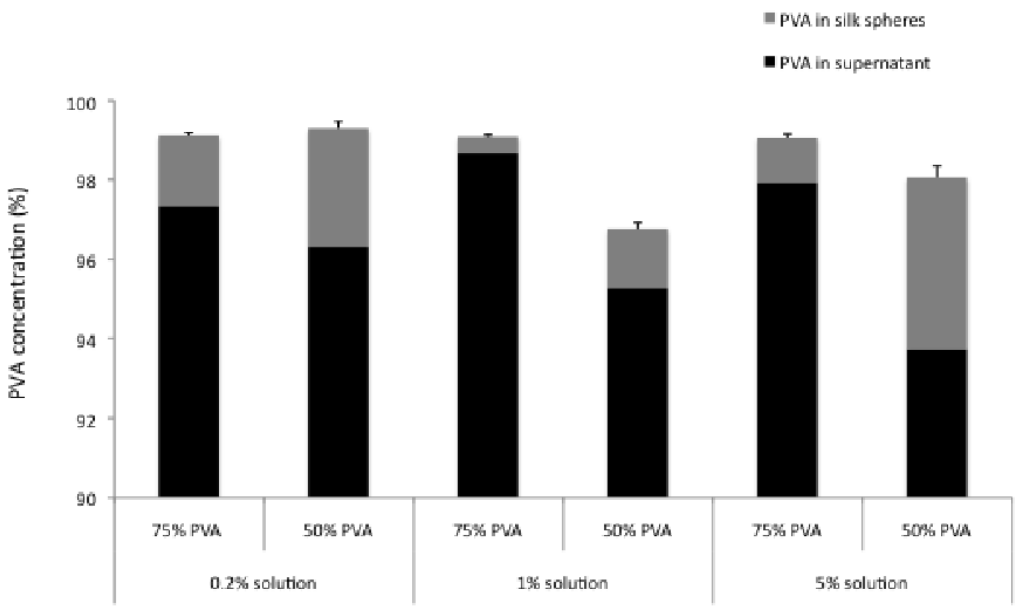

Figure 3.
Residual PVA determined in the supernatant fractions after silk spheres preparation (black columns) and in the silk spheres after protease XIV digestion (gray columns). Data represent the average ± S.D. (n = 3 - 4).

NIH-PA Author Manuscript

NIH-PA Author Manuscript

NIH-PA Author Manuscript

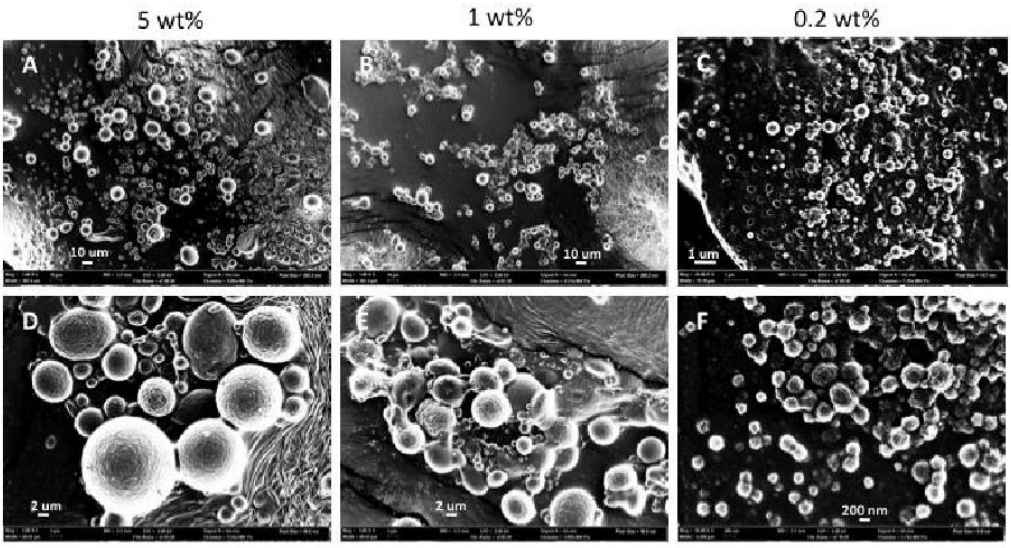

Figure 4.

Scanning electron microscopic images of silk spheres with size controlled by varying silk and PVA concentration. Silk/PVA weight ratio was 1/4. The samples of 5 and 1 wt% silk and PVA concentration were dominated by silk microspheres with a size range of 1 – 30 μm (A,B,D,E) whereas the samples of 0.2 wt% was dominated by nanospheres with a size lower than 400 nm (C,F). Upper panel shows low magnification images, scale bar = 10 μm in A,B to show multiple microspheres in general; 1 μm in C to show multiple nanospheres. Lower panel show high magnification images, scale bar = 2 μm in D,E; 200 nm in F to show detailed structure of nanospheres.

NIH-PA Author Manuscript

NIH-PA Author Manuscript

NIH-PA Author Manuscript

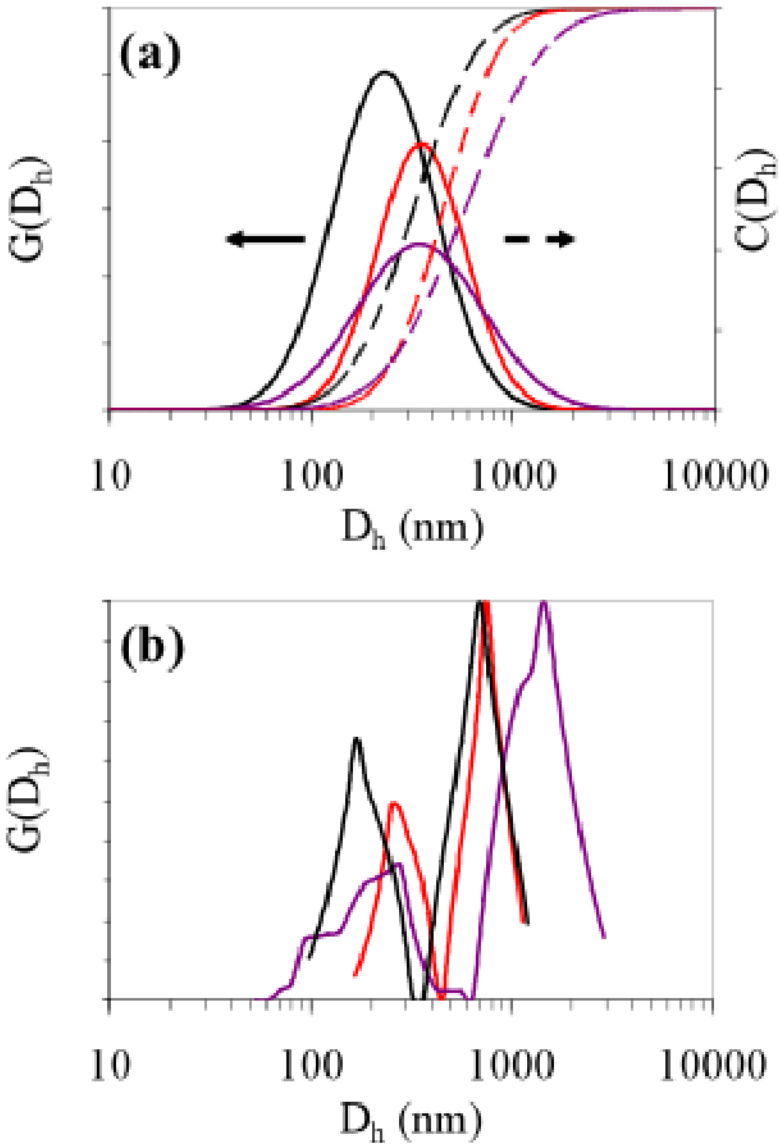

Figure 5.

Dynamic light scattering data obtained from silk spheres showing size control by varying silk and PVA concentrations and sonication, at a constant silk to PVA weight ratio of 1/4: **(a)** Probability densities ($G(D_h)$, solid lines) and cumulative distributions ($C(D_h)$, dashed lines) obtained from 0.2 wt% (red), 5 wt% (purple) and 5 wt% with 8 W sonication energy (black) samples using the cumulant analysis. **(b)** Hydrodynamic size distributions obtained from the same samples as in (a) using intensity-averaged exponential sampling.

NIH-PA Author Manuscript

NIH-PA Author Manuscript

NIH-PA Author Manuscript

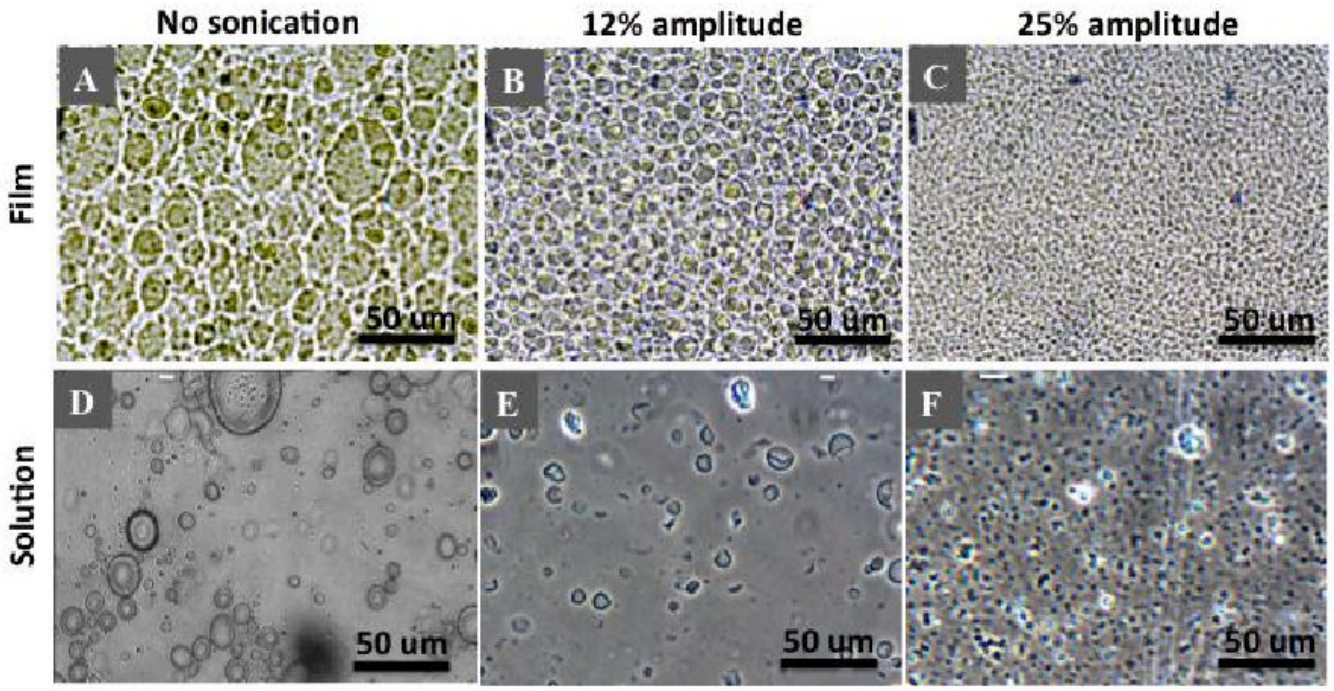

Figure 6.

Microscopic images of silk spheres with size controlled by applying ultrasonication on silk/PVA blend solution prior to casting film. The blend solution used had a concentration of 5 wt % and silk-PVA weight ratio of 1/4. The control sample without sonication contained silk spheres with a broad size distribution from nanometer to micrometer in both blend film (A) and water suspension (D). The sample sonicated with 12% energy output was dominated by microspheres with a size range of 5 – 10 μm in both blend film (B) and water suspension (E). The sample sonicated with 25% energy output was dominated by nanospheres in both blend film (C) and water suspension (F). Bar = 50 μm.

NIH-PA Author Manuscript

NIH-PA Author Manuscript

NIH-PA Author Manuscript

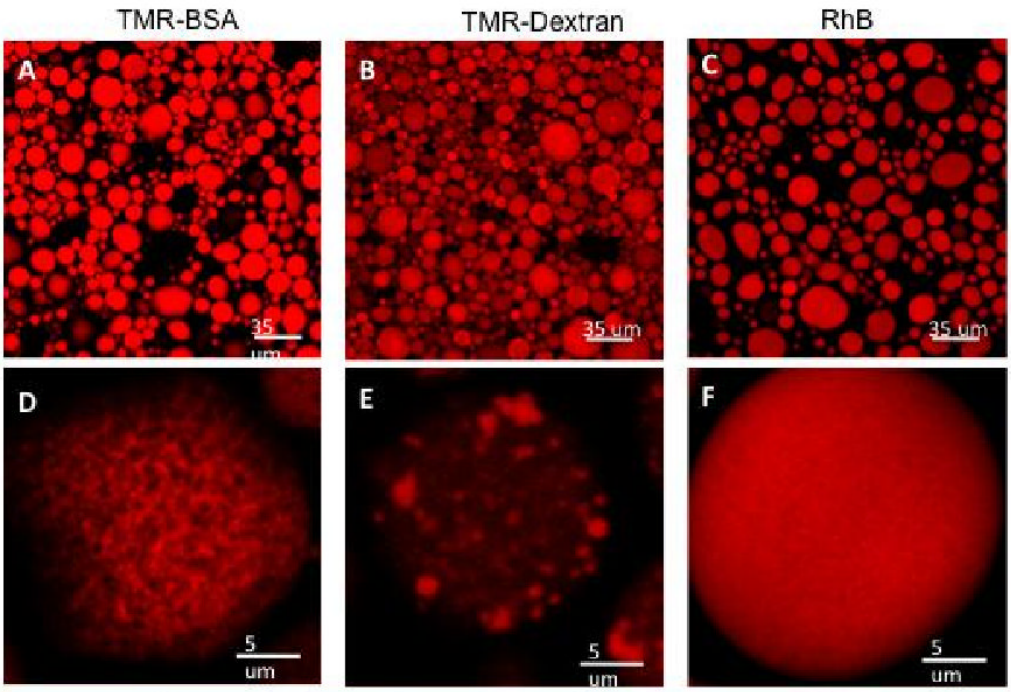

	Property	Initial amount (mg/mg silk)	Actual loading (mg/mg silk spheres)	Loading efficiency (%)
TMR-BSA	Hydrophobic Negative charge	0.01	0.00512	51.2
TMR-Dextran	Hydrophilic Neutral	0.01	0.00012	1.2
RhB	Hydrophobic Positive charge	0.01	0.00945	94.5

Figure 7.

Loading and distribution of model drugs in silk spheres. The concentration of silk and PVA used was 5 wt% and the weight ratio was 1/4. Model drugs, i.e., TMR-BSA, TMR-dextran and RhB, were pre-mixed with silk before blending in PVA. Confocal images were made on the spheres suspended in aqueous solution. A-C, low magnification images, bar = 35 μm. D-F, high magnification images, bar = 5 μm. The table below showed drug loading and loading efficiency determined by measuring the amount of drug remained in the supernatant fractions after centrifugation.

NIH-PA Author Manuscript

NIH-PA Author Manuscript

NIH-PA Author Manuscript

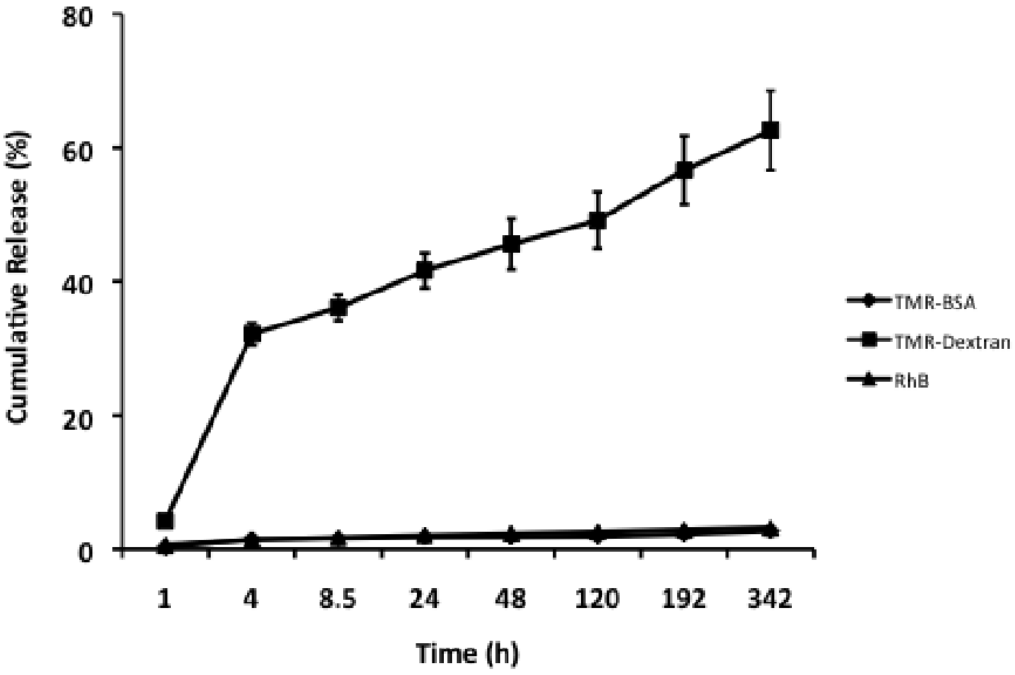

Figure 8.

Cumulative drug release from silk spheres. Silk spheres loaded with model drugs were prepared from silk/PVA blend films (silk and PVA concentration of 5 wt% and the weight ratio of 1/4). To determine drug release, the silk spheres were spun down at desired time points and the drug concentrations in the supernatants were measured. Diamonds – TMR-BSA release; Squares – TMR-dextran release; Triangles – RhB release.

NIH-PA Author Manuscript

NIH-PA Author Manuscript

NIH-PA Author Manuscript

Table 1
Beta-sheet content in silk spheres prepared from Silk/PVA blend films

Sample Number	Silk and PVA Ratio	Treatment	Beta-sheet Content (%)
1	1/4	Dissolve blend film in water	30
2	1/4	Stretch and dissolve blend film in water	28
3	1/4	Water anneal and dissolve blend film	30
4	1/4	Blend film prior to dissolution (control)	19
		Sonicate blend solution at 25% amplitude	42
5	1/4	Add 50% MeOH to blend solution	48
6	1/1	Blend film prior to dissolution (control)	27
		Dissolve blend film in water	28
7	1/1	Stretch and dissolve blend film in water	30
8	1/1	Water anneal and dissolve blend film	33

NIH-PA Author Manuscript

NIH-PA Author Manuscript

NIH-PA Author Manuscript

Table 2

Average sphere hydrodynamic diameters and polydispersities obtained using DLS cumulant analysis

Silk/PVA Concentration (wt%)	Sonication Amplitude (%)/Time (s)	D_h (nm)	PDI (a.u.)
5	None	578	0.68
1	None	536	0.56
0.2	None	452	0.29
5	12/30	308	0.4
5	25/30	322	0.4

NIH-PA Author Manuscript NIH-PA Author Manuscript NIH-PA Author Manuscript

Table 3

Summary of silk fibroin-based drug delivery systems

Silk delivery system	Preparation	Dimension	Drug loaded	In vitro drug release	Ref
Microspheres	Lipid-template	2-3 μm	Adenosine	14 days	[34]
			HRP	> 4 weeks	[13]
			BMP-2, IGF-I	> 14 days	[6]
	PVA blend film	5-10 μm	BSA	> 4 weeks	Present study
			Dextran	7 days	
			Rhodamine B	> 4 weeks	
	Spray-drier	5 μm	theophylline	N.D.	[19]
	Vibrational splitting of laminar jet	101-440 μm	Salicylic acid	1 day	[16]
			propranolol hydrochloride	20 days	
			IGF-I	> 7 weeks	
Nanospheres	PVA blend film	300-400 nm	Same as silk/PVA microspheres	Same as silk/PVA microspheres	Present study
	Bioengineer ed silk	300-400 nm	Plasmid DNA	N.D.	[35]
	capillary-microdot	< 100nm	Curcumin	> 8 weeks	[36]
	Acetone mix/ dialysis	35-125 nm	L-asparaginase	N.D.	[22], [37]
Film	Air-dry and Post-treatment	Micron thickness	NGF	> 3 weeks	[38]
		Micron thickness	Dextran, HRP, lysozyme	> 4 weeks	[12]
Layer-by-layer coatings	Coat substrate	Submicron thickness	Rhodamine B, Azoalbumin	> 2 weeks	[39]
	Coat drug tablet	N.D.	theophylline	> 8 hours	[40]
	Coat stents	6 layers	Heperin	N.D.	[41]
Porous sponge	Drug absorbed	300-400 μm pores	BMP-2	> 7 days	[42]
	Drug encapsulated	200-300 μm pores	IGF-I	> 4 weeks	[43]
Nano-fiber	Electro-spinning	Submicron diameter	BMP-2	N.D.	[44]

HRP = horseradish peroxidase; BMP-2 = bone morphogenetic protein 2; IGF-I = insulin-like growth factor I; BSA = bovine serum albumin; NGF = nerve growth factor

Biomaterials. Author manuscript; available in PMC 2011 February 1.